Aromaticity of Osmaacenes in Their Lowest-Lying Singlet and Triplet States

Slavko Radenković[1]* and Miquel Solà[2]*

[1]*University of Kragujevac, Faculty of Science, P. O. Box 60, 34000 Kragujevac, Serbia*

[2]*Institute of Computational Chemistry and Catalysis and Department of Chemistry, University of Girona, C/ M. Aurèlia Capmany, 69, 17003 Girona, Catalonia, Spain*

Abstract

The aromatic character of a series of osmaacenes in their lowest-lying singlet and triplet states was thoroughly examined by means of the magnetically induced current densities and multicentre delocalization indices (MCI). Both employed approaches agree that the osmabenzene molecule (**OsB**) in the S_0 state exhibits dominant π-Hückel-type aromatic character, with a small but nonnegligible amount of π-Craig-Möbius aromaticity. Contrary to benzene, which is antiaromatic in the T_1 state, **OsB** preserves some of its aromaticity in the T_1 state. In higher members of the osmaacene series in the S_0 and T_1 states, the central Os-containing ring becomes nonaromatic, acting as a barrier between the two side polyacenic units which, on the other hand, exhibit a significant extent of π-electron delocalization.

INTRODUCTION

Metallabenzenes represent a class of organometallic compounds characterized by the formal replacement of a CH unit in benzene by an isolobal transition-metal fragment.[1] Already in 1979, Thorn and Hoffmann[2] predicted that metallabenzenes might be synthesized as stable molecules. Only three years later, the first metallabenzene, an osmabenzene complex, was isolated and characterized by Roper *et al*.[3] Since then, the chemistry of metallaaromatics has attracted considerable attention from both theorists and experimentalists, and it has been suggested that this class of molecules might serve as a prospective candidate for novel aromatic functional materials.[1,4–9]

The aromatic characteristics of metallaaromatics have become a topic of intense debate.[5,7,10–13] It has been shown that studying the aromaticity in these systems is not a trivial task, and many new phenomena, which have not been previously detected in analogous organic compounds, appear.[5,7,14,15] For instance, aromaticity of monocyclic conjugated hydrocarbons and their heteroatom derivatives can be rationalized by several electron counting aromaticity rules.[16] On the other hand, even in the most simple monocyclic metallaaromatics there is an ongoing debate on how many electrons are involved in cyclic conjugation. In particular, it is not clear which d-atomic orbitals of the metal atom participate in π-electron delocalization.[17,18] Hoffmann and Thorn originally suggested that, as a result of the π-backdonation from the d_{xz} metal atomic orbital, metallabenzenes are characterized with six π-electrons.[2] Afterwards, it has been proposed that beside the d_{xz} orbital, also the d_{yz} metal atomic orbital significantly contributes to the π-electron delocalization, leading to the description of metallabenzenes as eight[1] and ten[5] π-electron systems. It should be noted that a combination of the d_{yz} atomic orbitals on the metal atom with the p_z atomic orbitals on the carbon atoms results in molecular orbitals of δ symmetry. The topology of such molecular orbitals motivated analysis of Craig-Möbius aromaticity in metallacycles.[5] Later on, Szczepanik and Solà using the electron density of delocalized bonds (EDDB)[19] concluded that in metallacycles both the d_{xz} orbital and the d_{yz} of the metal intervene in the electronic delocalization, and, therefore, metallacycles are hybrid Hückel and Craig-Möbius aromatic compounds with some metallacycles being more Hückel than Craig-Möbius and the other way round (see Scheme 1).[20] Another intriguing result obtained in studies of metallaaromatics, is that some of these systems were found to be aromatic in the lowest singlet state (S_0), as well as in their lowest-lying triplet excited state (T_1), which contradicts Hückel and Baird's rules.[16] This phenomenon was named

adaptive aromaticity.[21,22] In addition, some aromaticity indices, which can be successfully applied for polycyclic aromatic hydrocarbons, in the case of metallaaromatics can give wrong characterization of aromaticity. It has been demonstrated that NICS values calculated for osmabenzenes are dominantly influenced by the local currents around the metal atom.[23] Thus, the single point NICS index,[24–26] which is one of the most employed aromaticity measurements, is not a reliable tool for analyzing the metallabenzenes aromaticity.

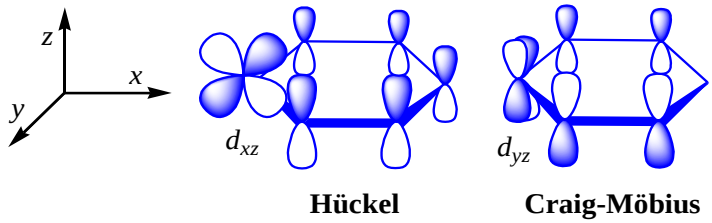

Scheme 1 Schematic representation of two different topologies of molecular π-orbitals involving *d*-orbitals. The Hückel (Craig-Möbius) molecular π-orbitals have an even (odd) number of nodes along the ring (not considering the node in the plane of the ring).

In 2003, Paneque *et al*. extended the range of metallaaromatics from monocyclic to polycyclic systems, completing the preparation of metallanaphthalene.[27] The first metallaanthracene was prepared by Wright and co-workers in 2017.[28] Theoretical investigations of the lowest-lying singlet and triplet states of acenes and phenacenes have been performed recently by some of us.[29] However, to our knowledge a similar study for polycyclic metallaaromatics having more than three condensed rings has not been carried out yet. In the present paper, we consider a series of linear polyacenes in which the transition metal fragment $[Os(CO)I(PH_3)_2]$ is included in the most central hexagonal ring. This metal fragment is a d^7 ML_4 and, therefore, it is isolobal with the organic CH fragment.[30] The general formula and notation of the studied molecules is depicted in Fig. 1. Since there are two distinct substituents on the Os atom, when the total number of hexagons is even, there are two possible isomers of this kind (for instance, **2,3-OsB** and **3,2-OsB**). It should be noted that, for each acene molecule, one can construct many more isomers containing the transition metal fragment at different locations. The influence of the position of the transition metal moiety on the aromaticity and stability of metallaaromatics has been recently examined.[7,10] The selection of the studied molecules was motivated by the work of An and Zhu who suggested that metallaacenes

with the transition metal group in the central ring can be produced from the corresponding metal-fluorenyl-type complex.[31] The starting compound in the examined series is osmabenzene **OsB** which has been much studied, but its aromaticity is not completely understood. Recently, Foroutan-Nejad *et al.* showed that **OsB** sustains diatropic (aromatic) magnetically induced currents.[23,32] In the same work, the authors emphasized the role of σ orbital contributions to the total current density and, based on magnetic criteria, describe **OsB** as a σ-type Craig-Möbius aromatic system.[23,32] It should be noted that for proper assessment of the aromatic characteristics in higher-multiplicity states one needs to employ more elaborated theoretical approaches.[33–35] In this work, the aromatic character of the studied molecules in their lowest-lying singlet and triplet states was examined by means of the magnetically induced current densities[36–38] and multicentre delocalization indexes (MCIs).[39] As will be shown in the following sections, our results do not confirm any relevant contributions from the σ orbitals to the aromaticity of **OsB** and, therefore, this system has to be classified as π-aromatic, more Hückel than Craig-Möbius aromatic in the ground singlet state and somewhat less aromatic in the lowest-lying triplet state.

It has been demonstrated that the magnetically induced current densities can provide more insightful description of the molecular aromaticity than the other magnetic indices,[36] such as the NICS-based techniques.[25] In the present paper the diamagnetic-zero version of the continuous transformation of origin of current density (CTOCD-DZ) method[40–43] was employed. Within the CTOCD-DZ approach, the total current density is partitioned into the occupied molecular orbitals contributions, which can be related to the respective virtual excitations to empty orbitals. Therefore, the employed method can provide a direct connection between the calculated induced current density and many important electronic structure details, such as molecular orbitals' occupancies, energies, and nodal properties.

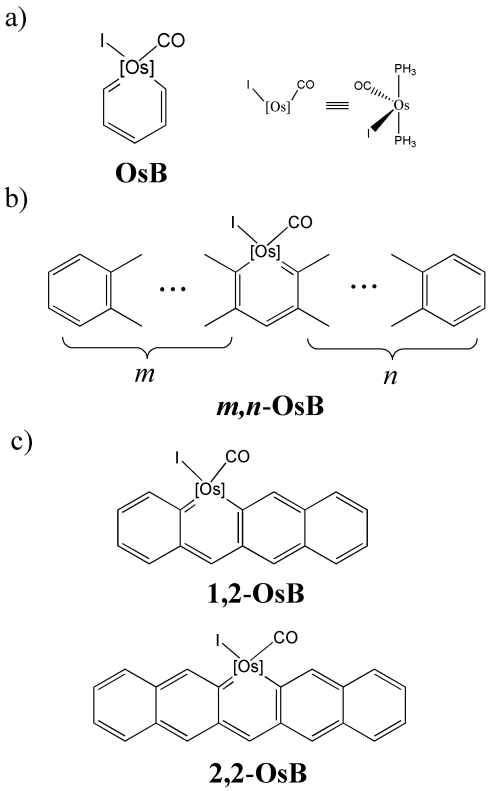

Fig. 1 Osmabenzene (**OsB**) and general formula of the examined molecules (a and b). According to the notation indicated, ***m,n*-OsB** has *m* and *n* hexagonal rings on the sides closer to I and CO groups, respectively, so the total number of rings equals $m + n + 1$. As an illustration two studied osmaacenes are shown (c): **1,2-OsB** and **2,2-OsB**.

COMPUTATIONAL DETAILS

Geometry optimizations and vibrational frequency calculations of the studied systems were performed at the BLYP-D3/TZP level of theory as implemented in the ADF (Amsterdam Density Functional) program.[44] The employed method includes London dispersion corrections introduced by Grimme *et al.* (D3),[45,46] as well as scalar relativistic effects through the zeroth-order regular approximation (ZORA).[47,48] Using the so-obtained optimized geometries, the current densities were calculated at the BLYP/def2-TZVP level of theory using the CTOCD-DZ method.[40–43] In all calculations, the external magnetic field was applied perpendicular to the plane that maximizes the projection area of the given molecule. The current densities were calculated and mapped 1 bohr above the surface, which approximately adopts the molecular shape. The computed current densities were visualized using the Paraview program.[49] In all current density maps, counterclockwise circulations represent diatropic (aromatic) current densities. The integrated bond

current strengths[50] were calculated using the disc-based quadrature scheme.[51] In this method, the bond current strength is calculated by numerical integration[52] of the current densities passing through a disc that perpendicularly bisects the given bond. The employed disc-based integration method has been recommended for nonplanar 3D structures, such as those having the ring, bowl or cage shapes.[51] Radius of the integration disc was set to the carbon van der Waals radius. Diatropic/paratropic currents were assigned to have positive/negative contributions to the bond current strength values.

The multicenter delocalization index (MCI)[53,54] was employed to quantify the extent of cyclic electron delocalization in individual hexagonal rings of the examined molecules. The MCI can be calculated using different partitioning schemes.[39,55–57] In this work, the natural atomic orbital (NAO) density matrices obtained from NBO analysis[58] were used to calculate MCI. The NAOs form an orthonormal basis, and in the case of hexagonal rings, the MCI can be computed in the following way:

$$MCI = \sum_{i\in A}\sum_{j\in B}\sum_{k\in C}\sum_{l\in D}\sum_{m\in E}\sum_{n\in F}\sum_{q} P^{\alpha}_{ij}P^{\alpha}_{jk}P^{\alpha}_{kl}P^{\alpha}_{lm}P^{\alpha}_{mn}P^{\alpha}_{ni} + \sum_{i\in A}\sum_{j\in B}\sum_{k\in C}\sum_{l\in D}\sum_{m\in E}\sum_{n\in F}\sum_{q} P^{\beta}_{ij}P^{\beta}_{jk}P^{\beta}_{kl}P^{\beta}_{lm}P^{\beta}_{mn}P^{\beta}_{ni} \qquad (1)$$

where P^{α} and P^{β} are alpha and beta NAO density matrices, respectively, the first six sums go over all NAOs (*i*, *j*, *k*, *l*, *m* and *n*) centered on atoms A, B,…, F, respectively, and the last sum goes over all possible permutations (*q*) for each selection of the six NAOs. The NBO analysis was performed at the BLYP/def2-TZVP//BLYP-D3/TZP level of theory using the Gaussian 09 program.[59]

The extent of the deviation from planarity for examined molecules was quantified by means of the brute-force planarity index (BFPI).[60] The BFPI is calculated by finding a plane *Π* which minimizes the distances of all atoms in a molecule from *Π*. The BFPI is then given as the average distance of all atoms in the given molecule from the optimal plane *Π*. Calculations of current densities, bond current strengths, MCI, and BFPI were performed using in house FORTRAN programs. More information on the software can be found in our previous papers.[60,61]

RESULTS AND DISCUSSION

The optimized geometries of the studied molecules in their lowest-lying singlet (S_0) and triplet (T_1) states are shown in Fig. S1 in the supporting information. **OsB** exhibits a planar six-membered ring in the S_0 and T_1 states. In the two studied osmanaphthalenes (**0,1-OsB** and **1,0-OsB**) deviations from planarity are observed, which are more pronounced in **0,1-OsB** where the CO group points toward the central part of the molecule. The calculated BFPI values shows that

both osmanaphthalenes become almost planar in the triplet state (Table 1 and Fig. S1). In all other molecules the Os group is included in nonterminal rings, having two neighboring hexagons. As can be seen from the optimized geometries in both spin states (Fig. S1), the molecular nonplanarity originates from deformations of the central ring containing the Os-group, while the side polyacenic subunits preserve their planarity. Thereafter, the BFPI was calculated based on the spatial coordinates of the six atoms involved in the Os-containing ring ($BFPI_{Os6MR}$ in Table 1). Based on the $BFPI_{Os6MR}$ it is evident that the planarity deviations of the central Os-containing ring are practically not affected by the molecular size. On the other hand, the $BFPI_{total}$ is significantly influenced by the size of molecules, which reveals some limitations of this planarity descriptor. The $BFPI_{Os6MR}$ results show that the distortion of the central Os-containing hexagons is more pronounced in the T_1 than in S_0 state, except for **4,4-OsB**. If one compares two isomers having the same number of hexagons, in the S_0 state the one with the CO group oriented towards the molecular center show larger planarity deviation than that having the I atom pointing towards molecule's center. The opposite regularity is observed for the T_1 state optimized geometries.

Table 1 also displays the singlet-triplet energy gaps (ΔE_{ST}) of the examined molecules, which were calculated as the energy difference between the T_1 and S_0 optimized geometries obtained at the BLYP-D3/TZP level of theory. The so-obtained adiabatic singlet-triplet energy gaps decrease with increasing number of hexagons, but the ΔE_{ST} quantity stays positive-valued for the whole series. This result revealed that the studied molecules are more stable in their singlet state than in the corresponding triplet state. The same trend was reported for acenes, with larger ΔE_{ST} values for shorter acenes as compared to osmaacenes of same size and similar ΔE_{ST} values for longer (osma)acenes.[29] In the case of two osmaacenes isomers having the same number of rings, the larger ΔE_{ST} value is found for the isomer having the I atom oriented towards the center of the given molecule. This is not the case for the two naphthalene derivatives in which, unlike the other molecules, the Os fragment is included in the terminal ring. It has been shown that longer acenes exhibit a biradical character in their singlet states, which can be properly treated within the unrestricted symmetry-broken DFT approach.[29,62,63] In order to analyze the biradical character in the S_0 state of the studied systems, the molecular geometries were also optimized using the unrestricted symmetry-broken BLYP method, but the obtained structures coincide with those obtained with the restricted formalism, thus indicating that the ground state of all systems studied here is the singlet closed-shell. In addition, for **4,4-OsB**, which exhibits the smallest ΔE_{ST} value in

the series, the first quintet state was found to be 26.7 kcal/mol above the first triplet state at the BLYP/def2-TZVP level. This means that long osmaacenes, in contrast to acenes, offer low ΔE_{ST} values with relatively good stability. A detailed examination of the molecular orbitals showed that the T_1 state of the examined osmaacenes is a $\sigma\pi^*$ state derived by the excitation of an electron from σ to π^* orbital. A characteristic feature of the $\sigma\pi^*$ state is that the number of π_α and the number of π_β differ by one.

Table 1 Singlet-triplet energy gaps (ΔE_{ST}, in kcal/mol) at the BLYP-D3/TZP level. BFPI (in Å) obtained for the carbon-Os-atom skeleton ($BFPI_{total}$), and BFPI for the Os-containing six-membered rings ($BFPI_{Os6MR}$) based on the BLYP-D3/TZP optimized geometries in the S_0 and T_1 states.

Compound	ΔE_{ST}	$BFPI_{total}$		$BFPI_{Os6MR}$	
		S_0	T_1	S_0	T_1
OsB	32.64	0.000	0.000	0.000	0.000
0,1-OsB	34.77	1.203	0.185	0.898	0.150
1,0-OsB	26.01	0.759	0.026	0.614	0.023
1,1-OsB	25.62	2.528	2.381	1.167	1.192
1,2-OsB	18.59	2.936	2.867	1.198	1.292
2,1-OsB	22.45	2.745	2.906	1.157	1.376
2,2-OsB	16.44	3.754	3.909	1.184	1.373
2,3-OsB	11.31	4.272	4.252	1.197	1.316
3,2-OsB	13.80	4.192	4.462	1.178	1.391
3,3-OsB	10.08	4.864	5.156	1.192	1.370
3,4-OsB	6.38	5.393	5.268	1.196	1.216
4,3-OsB	8.43	5.365	5.809	1.190	1.377
4,4-OsB	5.54	5.865	5.720	1.196	1.175

Total current density plots calculated 1 bohr above the ring plane of **OsB** show that this molecule in the S_0 and T_1 states exhibits a diatropic (counterclockwise) global circulation inside and paratropic (clockwise) circulation inside the molecular ring (Fig. 2a and 2d). In both plots, there are also very strong local circulations around the Os and I atoms. More information on the nature of the induced currents can be obtained from the integrated bond current strengths (Table 2) and bond current strength profiles (Fig. 3). For the sake of comparison, the bond current strengths were calculated for benzene in its ground state and its T_1 state at the same level of theory and using the same integration surfaces (ground state: I^{total} = 12.0 nA/T; I^{π} = 10.9 nA/T; I^{σ} = 1.2 nA/T; T_1 state: I^{total} = -27.0 nA/T; I^{π} = -28.0 nA/T; I^{σ} = 1.0 nA/T). The bond current strength profiles are obtained by a stepwise integration using thin slices of the integration surface used to

obtain the bond current strength. The calculated bond current strengths and bond current strength profiles revealed that in **OsB** in both spin states the π-electrons solely contribute to the total diatropic current density. The intensity of π-electron currents in the S_0 state of **OsB** is about half of that in benzene, while the magnitude of π-electron currents in the T_1 state (a $^3\sigma\pi^*$ state) is about 1/3 of that in the S_0 states. A similar behavior has been reported for the $^3n\pi^*$ state of a number of heterocycles.[64] These results have been rationalized considering the increase in one π-electron and taking into account the Mandado's $2n+1$ rule for aromaticity of separate spins.[65]

In the case of σ-electron subsystem of **OsB**, the situation is more complicated. There are two separate σ-electron current circulations: paratropic inside and diatropic outside the molecular rings (Figs. 2 and 3). The bond current strengths of σ-electrons show that the intensities of these two components are very similar, which results in very small net diatropic ring current strength of 0.4 nA/T in the S_0 state. It should be noted that the σ-electron currents were also plotted 1 bohr above the molecular plane in order to avoid possible visual confusions coming from the strong localized σ electron currents. In the T_1 state, although both paratropic and diatropic contributions of σ-electrons are somewhat reduced relative to the S_0 state, the net diatropic σ-electron bond current strength is increased to 1.1 nA/T. The presented current density analysis showed that **OsB** in the S_0 state has aromatic character, while the T_1 state preserves only a small part of the S_0 state aromaticity. Similar behavior has been found in some osmapyridine complexes characterized as adaptive aromatic, since these systems are aromatic in the lowest singlet and triplet states.[21,66]

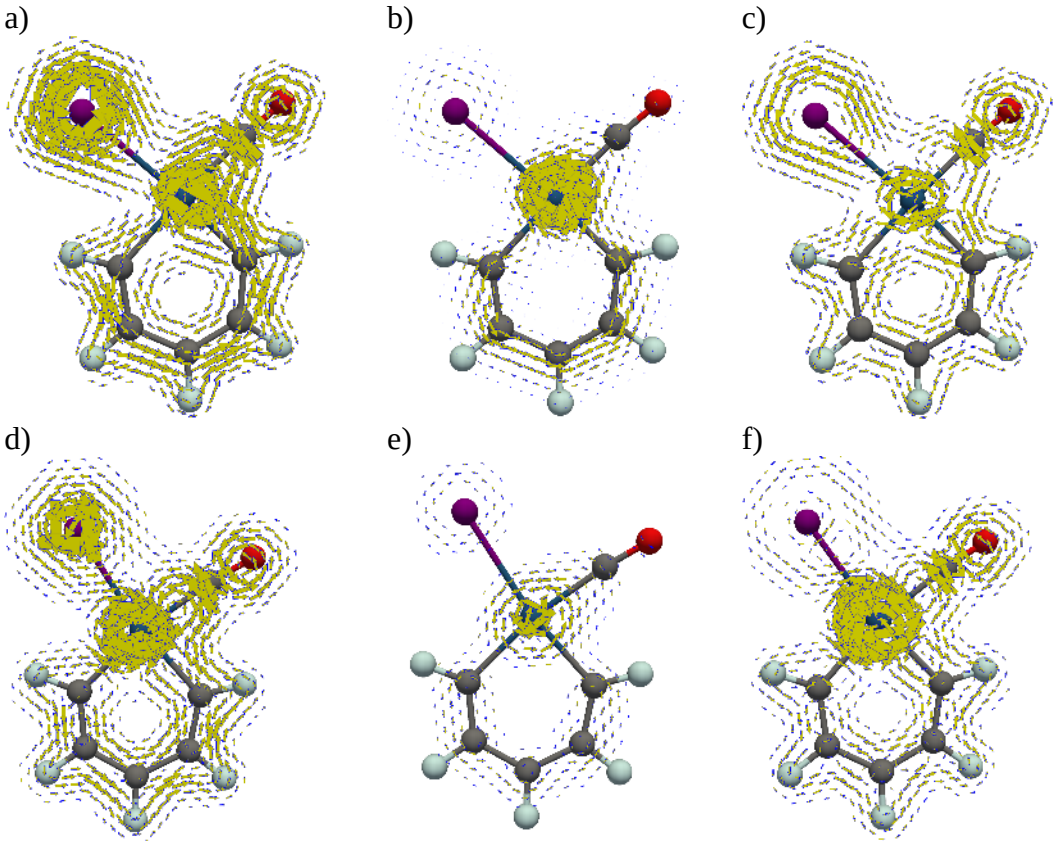

Fig. 2 Magnetically induced current density plotted in the plane 1 bohr above the molecular plane of **OsB** in the S_0 state (top) and the T_1 state (bottom): total (a and d), π (b and e) and σ (c and f). For the sake of clarity, the PH_3 groups were not displayed.

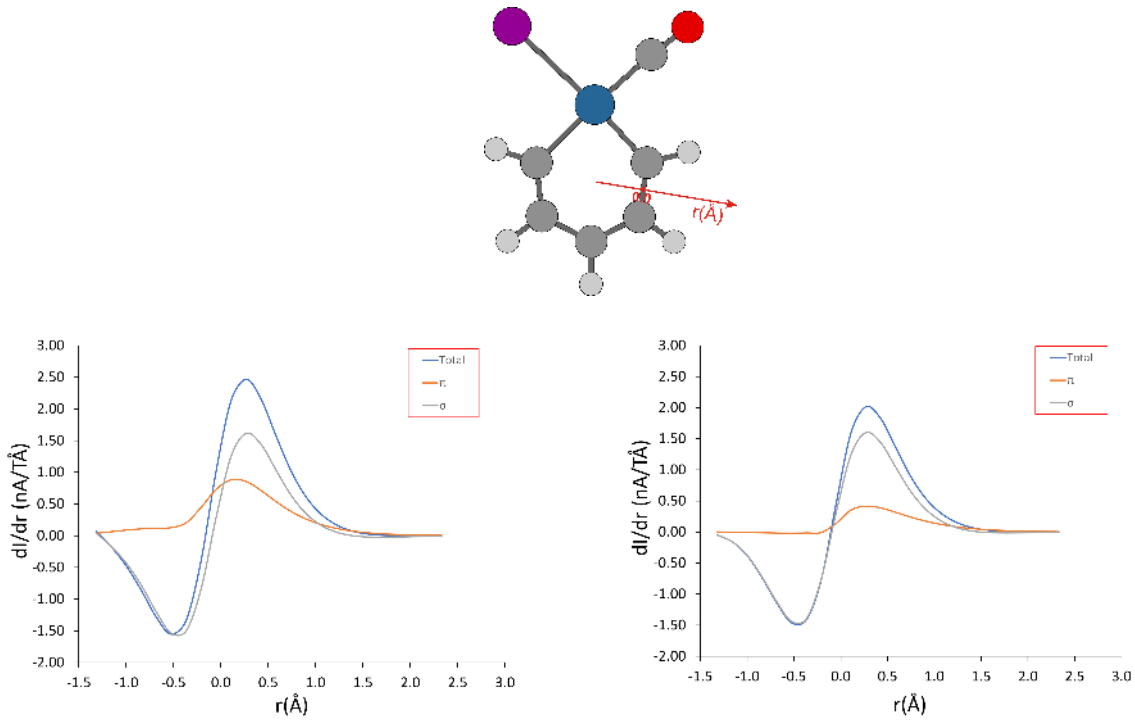

Fig. 3 The bond current strength profile along the arrow passing through a selected C-C bond of **OsB** in the S_0 (left) and T_1 (right) state. The arrow origin is at the center of the considered bond. Diatropic current is assumed to be positive.

Table 2 Integrated ring current strengths (*I*, in nA T^{-1}) of **OsB** in its S_0 and T_1 states. The ring current strength was calculated as the average of the bond current strengths of all bonds in the given six-membered ring.

I	S_0	T_1
Total	4.8	2.4
$Total_{\alpha}$	2.4	0.8
$Total_{\beta}$	2.4	1.6
π	4.4	1.4
π_{α}	2.2	0.5
π_{β}	2.2	0.8
σ	0.4	1.1
$\sigma^{diatropic}$	7.3	6.4
$\sigma^{paratropic}$	-6.9	-5.3

The present current-density-based analysis revealed that in **OsB** in the S_0 state 91.7% of total diatropic current arises from the π electrons and the remaining nonnegligible 8.3% comes from the *σ* electrons. On the other hand, a recent work of Foroutan-Nejad *et al.* suggested that **OsB** in the S_0 sate sustains a strong σ-current density circulation.[23,32] As can be seen from the bond-current-strength-based results (Table 2 and Fig. 3), the σ electrons induce very strong currents with opposite tropicity inside and outside the molecular ring, giving very weak net ring current strength. On the other hand, in the T_1 state the total diatropic current have 58.3% and 41.7% of the π and σ electron contributions, respectively. In order to provide more details on the π-electron currents in **OsB**, the bond current strengths were partitioned into contributions of individual π-orbitals (Fig. 4). By defining π-orbitals as those antisymmetric with respect to reflection in the molecular plane, 12 π-electrons were found in the S_0 state of **OsB**. The diatropic current in the S_0 state mainly arises from the contribution of MO61, MO58, and MO56, while the MO62 has a significant paratropic contribution. Nodal properties of MO58 indicate that this orbital gives rise to Hückel-type aromaticity, while MO61 and MO56 solely contribute to Craig-Möbius aromaticity. Although the MO62 has a mixed contribution of the Os d_{xz} and d_{yz} orbitals, this MO dominantly provide Craig-Möbius-type aromaticity. Therefore, the MO decomposed bond current strengths shown in Fig. 4 reveal that **OsB** in the S_0 state exhibits dominant Hückel-type aromaticity. In the T_1 state there are 7 π_α and 6 π_β electrons, revealing the excitation from the *σ*-electron subsystem of the S_0 state. Among π_α MOs in the T_1 state the most dominant is the paratropic contribution of MO64 which is balanced by diatropic contributions of MO63 and MO61. All these π_α MOs (MO61, MO63, and MO64) contribute to the Craig-Möbius-type (anti)aromaticity. Similar to the S_0 state, the π_β MO62 in the T_1 state has relatively strong paratropic contribution, but the rest of π_β MOs give weaker diatropic contribution, which results in significantly less intensive π_β current strength than in the S_0 state.

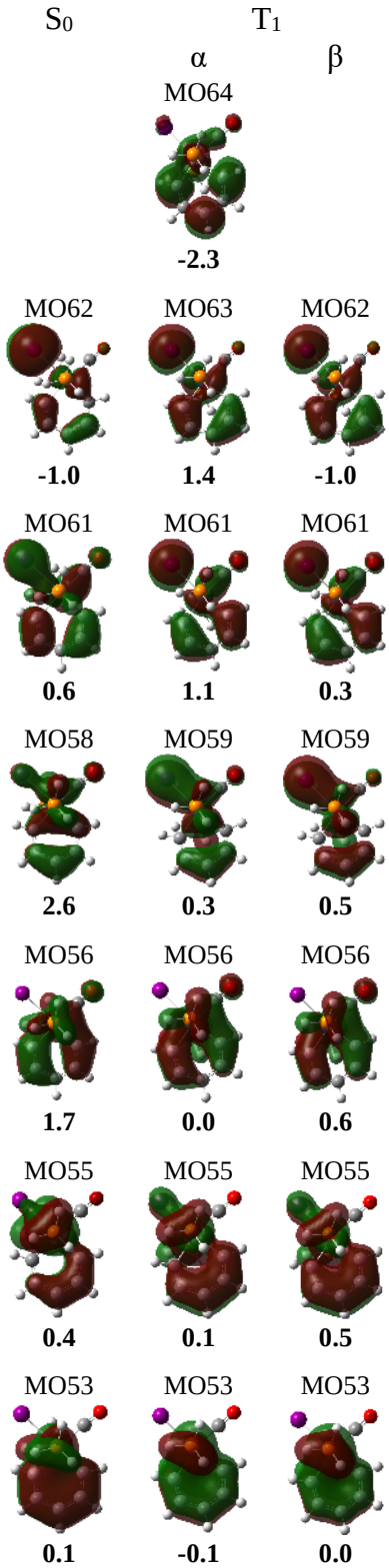

Fig. 4 Occupied π molecular orbitals (MOs) of **OsB** and their contribution to the ring current strength in nA T^{-1} (bold numbers).

The aromatic character of the studied molecules can be further analyzed based on the calculated MCI values (Table 3). The extent of cyclic delocalization in **OsB** is much more pronounced in the S_0 than in the T_1 state, but again the MCI value in the S_0 state of **OsB** is less than a half of that in benzene (for benzene at the same level of theory MCI = 0.0490 e). This finding supports the results of the current-density-based analysis. Spin-separated MCI values demonstrate that in the T_1 state the β-spin-component is reduced in comparison to that of the S_0 state (half of the S_0 state MCI value is 0.0105 e), while the α-spin-component has very small negative contribution, like that found in a number of antiaromatic systems. In the σπ* transition to generate the T_1 state, the number of β-electrons remains the same and, therefore, we expect β-spin-component to change less than the α-spin-component that increases the electron counting by one.[65] Eq. 1 provides a straightforward way to analyze contribution of individual atomic orbitals (AOs) to the MCI value. For instance, to obtain contributions of π-electrons in benzene, one needs to restrict the summation in Eq. 1 to the p_z NAOs located on the C atoms (assuming that the benzene ring lies in the *xy*-plane). In this way, for benzene one gets π-MCI = 0.0489, which clearly shows that more than 99% of the total MCI comes from π-electron contribution. The interpretative power of NBO analysis combined with the MCI method can provide a new insight into contributions of the individual *d*-metal orbitals in cyclic π-conjugation of metallabenzenes. The p_z NAO contributions to the total MCI is very small in the S_0 **OsB**, which is expected since in this way no *d*-orbitals on the Os atom are included. However, joint contribution of the p_z and d_{xz} NAOs of the Os atom (assuming that the six-membered ring lies in the *xy*-plane, and that the Os atom and the C atom at the *para* position lie on the *x* axis, Scheme 1) can provide 91% of the total MCI. This is in line with original suggestion of Thorn and Hoffmann[2] that only d_{xz} metal orbital is involved into π-electron delocalization in the S_0 state of **OsB** (Hückel aromaticity). However, the presented MCI-based analysis showed that the d_{yz} metal orbital have much less important role in cyclic delocalization, which is the remaining nonnegligible 9% of the total MCI (Craig-Möbius aromaticity). The NAO-decomposed MCI values demonstrate that in the T_1 state the π_β-electrons show that exhibit identical proportions of Hückel and Craig-Möbius aromaticity (92% and 8%, respectively) as in the S_0. On the other hand, within π_α-electrons in the T_1 **OsB** involvement of the Os d_{yz} orbital in π-electron conjugation gives rise to (Craig-Möbius) antiaromaticity. The data from Table 3 reveal very weak aromatic character of π_α-electrons in the T_1 state, which comes from 48% of Hückel aromatic and 52% of Craig-Möbius antiaromatic contributions. Interestingly, although

the Os d_{xz} and d_{yz} orbitals have different roles in cyclic electron delocalization, the natural population analysis (NPA) showed that these two atomic orbitals have very similar occupancies for both S_0 and T_1 states (Table S1).

Table 3 MCI values and their α and β electron components for the S_0 and T_1 states of **OsB** (units are electrons).

	S_0	T_1		
		α + β	α-component	β-component
Total	0.0210	0.0047	-0.0006	0.0053
π (contribution from p_z NAOs)	0.0011	0.0014	0.0011	0.0003
π (contribution from p_z and d_{xz} NAOs)	0.0192	0.0061	0.0012	0.0049
π (contribution from p_z, d_{xz} and d_{yz} NAOs)	0.0209	0.0046	-0.0006	0.0052

Before continuing with analyzing aromaticity of higher Os-acene derivatives, first the spin-density distribution in the studied systems in their T_1 states will be discussed (Fig. 5). The unpaired electrons are preferentially located in the Os-fragment-containing ring of the studied molecules. The most intensive spin densities are always found at the [Os] group, and at the carbon atoms at the *para* position within the same ring. Within the [Os] group the spin density is mainly shared between the Os and I atoms. Scheme 2 describes the pattern of the spin density distribution in the T_1 state of the studied osmaacenes, by showing that the most outer rings preserve their aromatic character, while the central rings can be described by diradical antiaromatic Baird configurations. If the number of hexagons is odd (even), the electronic configuration of the central rings is represented as a resonance between antiaromatic Baird π-doublets, π-dectects and π-octadectets (π-sextets and π-tetradectets). The normalized weights of antiaromatic Baird resonant structures (Table 4) have been obtained based on the NBO spin density values using the procedure described in the recent paper.[29] The localization of spin-density in the T_1 state of acenes follows a very similar shape.[29] The main difference is that in osmaacenes the small antiaromatic Baird configurations (π-doublets and π-sextets) have higher weights than in the corresponding acenes. This in line with more pronounced ability of the [Os] fragment to "localize" the unpaired electrons.

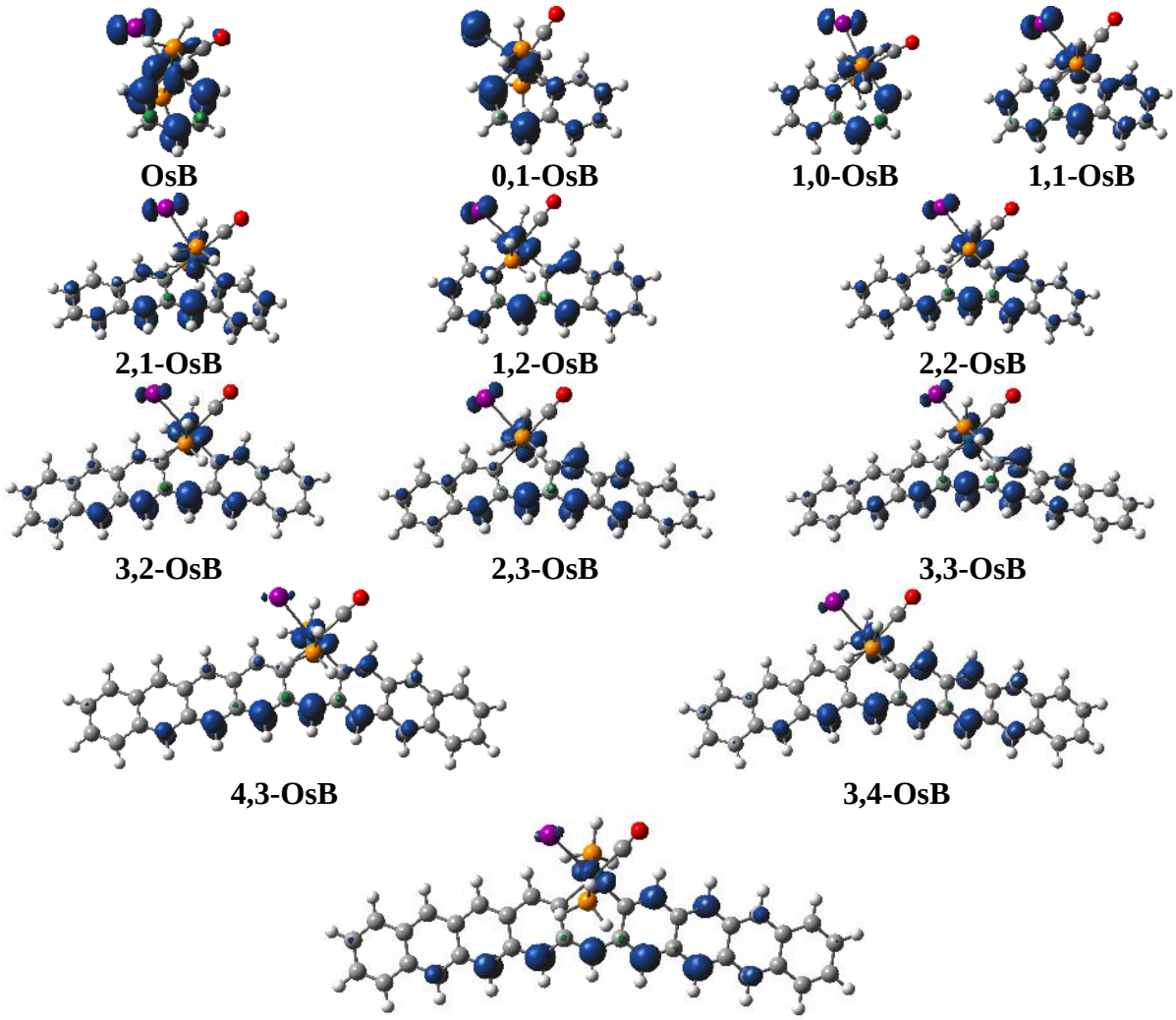

Fig. 5 Spin density maps plotted on isosurfaces of ±0.005 a.u.

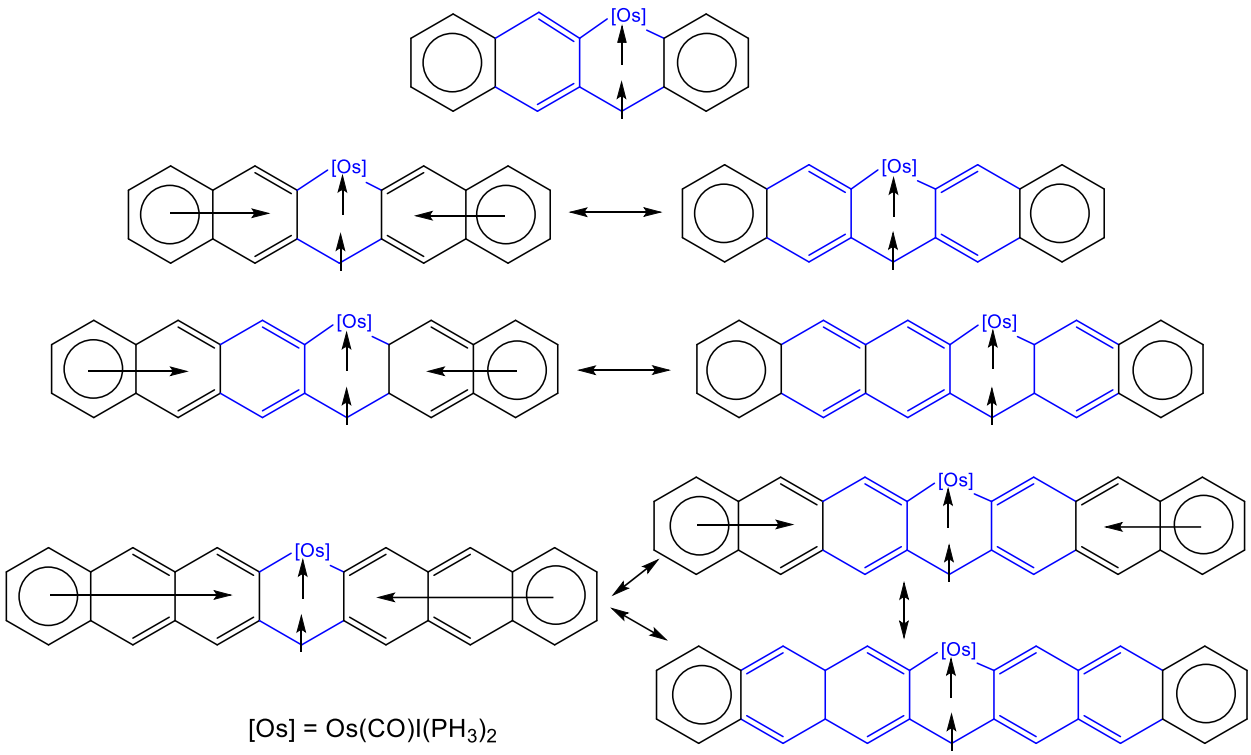

Scheme 2 The most relevant resonance structures for T_1 states of some of the systems studied with aromatic Clar π-sextets depicted with a circle and in blue the antiaromatic Baird π-doublets, π-sextets, π-dectets, π-tetradectets and π-octadectets.

Table 4 Weights for antiaromatic Baird's π-doublets, π-sextets, π-dectets, π-tetradectets, and π-octadectets in osmaacenes in their T_1 states.

Compound	Doublet	Sextet	Dectet	Tetradectet	Octadectet
1,1-OsB	100				
1,2-OsB		100			
2,1-OsB		100			
2,2-OsB	43		57		
2,3-OsB		46		54	
3,2-OsB		41		59	
3,3-OsB	28		18		53
3,4-OsB		33		67	
4,3-OsB		33		67	
4,4-OsB	14		13		73

The aromaticity of higher members of the studied series was based on the total current density maps and bond current strengths (Figs. 6 and S2) and the MCI values (Figs. 7 and S3). As

shown above, the total bond current strengths are dominated by the π-electron contributions. For the T_1 states, the calculated bond current strengths were dissected into α- and β-electron contributions. As a general regularity it was found that in both spin states the current density intensities within the Os-containing rings is significantly reduced relative to all other rings of a given molecule. For Os-acenes with fewer than 5 hexagons the current density intensities are much more pronounced in the S_0 than in the T_1 states. However, for higher members of the examined series this is not the case, and the current density flow around the terminal rings is even more significant in the T_1 than in the S_0 states. In comparison to **OsB**, all osmabenzene rings of the rest of studied osmaacenes have reduced diatropic current density flows in both S_0 and T_1.

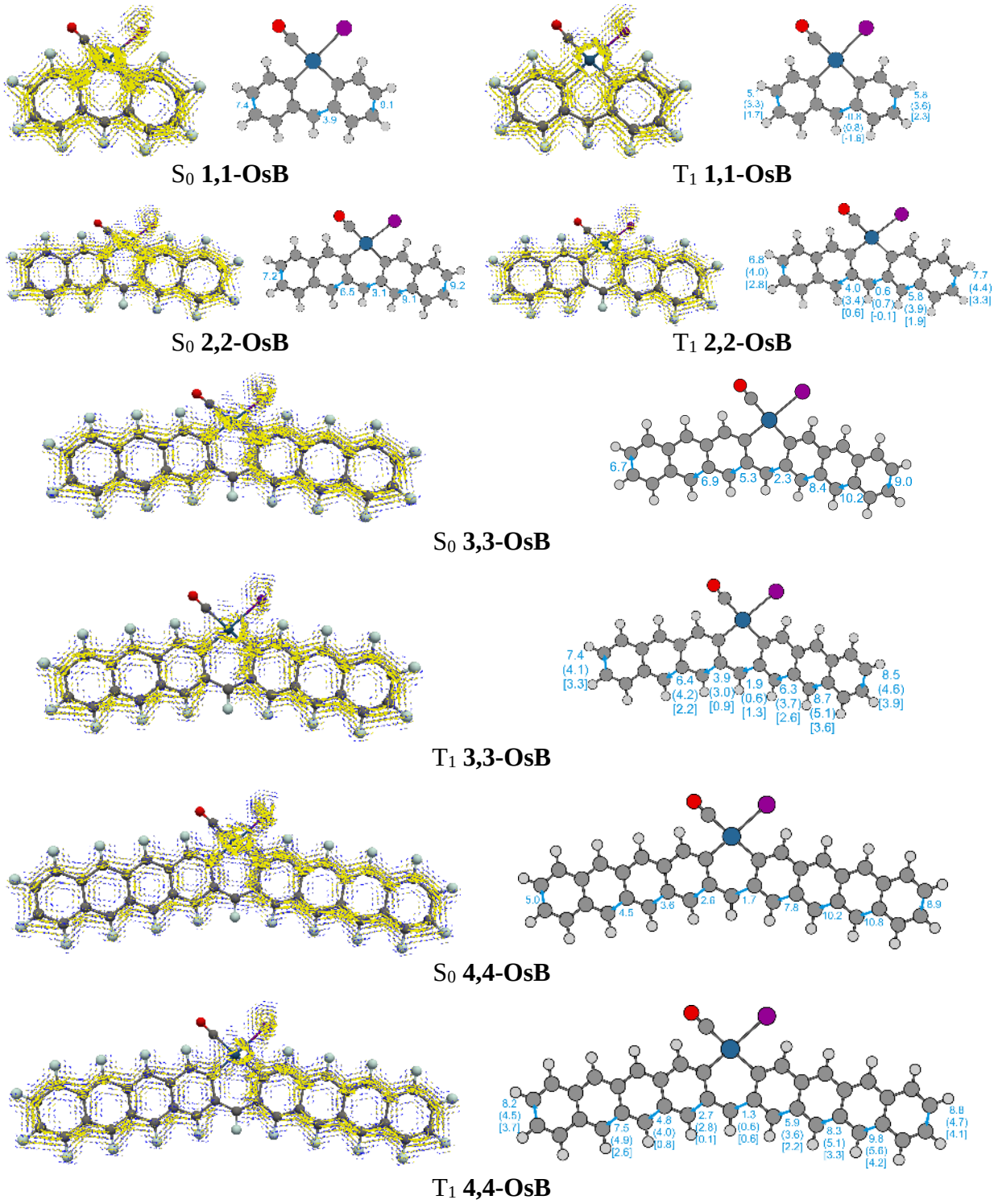

Fig. 6 Current density maps (left) and bond current strengths (right, in nA/T) of selected bonds. For the T_1 state the bond current strengths are divided into α- and β-electron contributions (in parentheses and square brackets, respectively). Current density maps of the other compounds studied are available in the ESI (Fig. S2).

Based on the MCI vales, in the S_0 state, the aromatic character of the Os-containing rings becomes reduced with increasing number of hexagons. On the other hand, in the S_0 state of all molecules the rings without the Os-fragment have a significant aromatic character that increases going from the central rings to the outer rings. This is in line with the planarity analysis provided above, which showed that only the Os-containing rings show important deviations from planarity. Thus, in the S_0 state, the Os-containing rings lose their planarity, and consequently part of their aromaticity, while the rest of molecule preserves the aromatic characteristics. The calculated MCI values show very similar trend in the T_1 states of the explored molecules. The Os-containing rings in the T_1 state show more significant deviations from planarity, and additionally, the unpaired electrons are located in these rings (Fig. 5 and Scheme 2). Therefore, in the T_1 states, the Os-containing rings are characterized with very small MCI values. Another characteristic features of the calculated MCI values, is that the Os-containing rings is always less aromatic in the T_1 than in S_0 state, while the opposite is generally found for all other rings in the given molecule. As found for acenes, osmaacenes in the T_1 are characterized by two external more aromatic six-membered rings and less aromatic central rings (see Scheme 2). One of the present authors demonstrated that the wrong long-range behavior of the conventional density functionals, such as BLYP, can give a significant overestimation of the extent of cyclic delocalization in linear acenes.[67] In order to assess the effect of the long-range exchange corrections in calculations of the MCI values, the ωB97xD functional[68] was employed. For **1,1-OsB** in the S_0 and T_1 states the BLYP and ωB97xD functionals provide numerically very similar MCI values (Fig. S4), suggesting that the more elaborated treatment of the long-range exchange contributions is not needed for a proper quantification of the π-electron delocalization in the examined molecules.

To estimate the spin-orbit effect on the intensity of electron cyclic delocalization, the geometry optimization was performed with the spin-orbit relativistic corrections incorporated through the ZORA approximation, as implemented in the ADF programme. The obtained MCI vales for **1,1-OsB** show that inclusion of the spin-orbit effect decreases the aromaticity in the T_1 state, whereas in the S_0 state this effect was found to be minute (Fig. SS). This is in agreement with previously obtained results.[69,70]

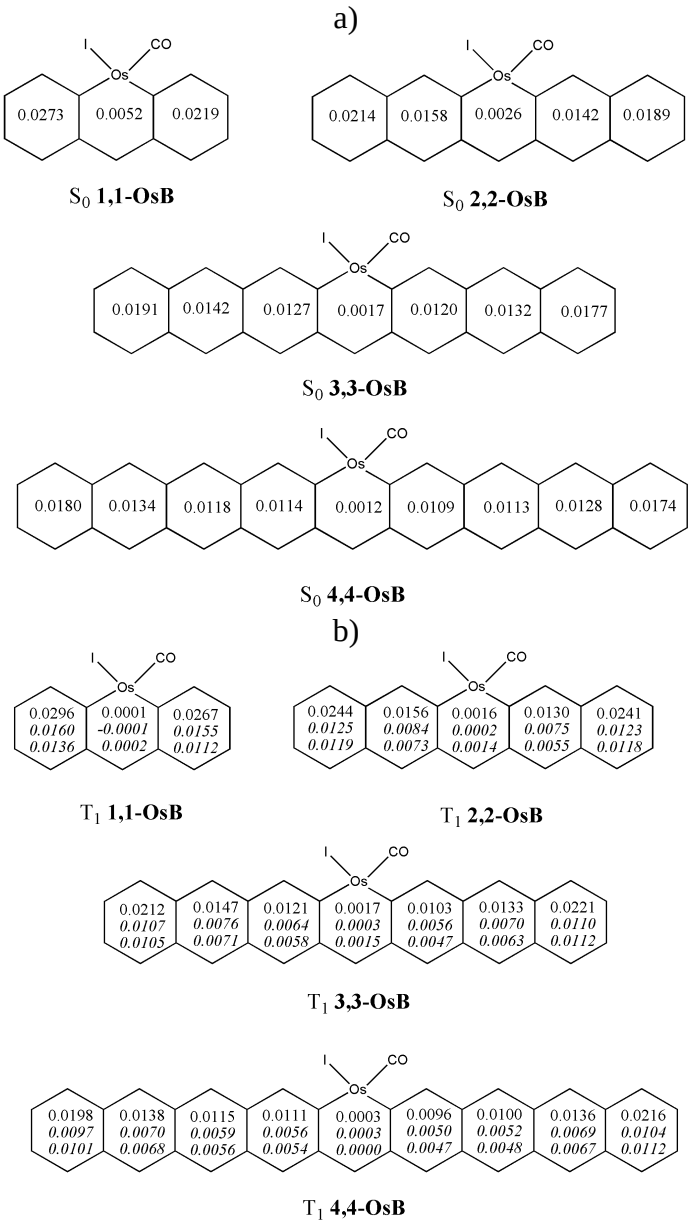

Fig. 7 MCI values (units are electrons) of selected molecules in their S_0 (a) and T_1 (b) states. For the T_1 state the MCI values are divided into α- and β-electron contributions (italic numbers). As a reference, for ground state benzene at the same level of theory MCI = 0.0490. MCIs of the other compounds studied are available in the ESI (Fig. S3).

CONCLUSIONS

Motivated by a recent theoretical investigations of the lowest-lying singlet and triplet states of acenes and phenacenes,[29] in this work we studied the aromatic character of a series of osmaacenes by means of the magnetically induced current densities and MCIs. The BLYP-D3/TZP adiabatic singlet-triplet energy gaps revealed that the studied molecules exhibit singlet ground states. The singlet-triplet energy gap decreases with the increase in the size of the osmaacenes, but stays positive-valued for the whole studied series. We found that osmaacenes lose their planarity due to deformations of the central ring containing the Os-group, while the side polyacenic subunits preserve their planarity. The planarity deviations of the central Os-containing ring are not dependent on the molecular size and are found to be more pronounced in the T_1 than in the S_0 state of the examined molecules.

The current-density-based analysis revealed that **OsB** in the S_0 state sustains relatively intensive diatropic circulations, which are dominated by the π electrons contribution (> 90%). Our findings contradict the results of a recent work of Foroutan-Nejad *et al.* suggesting that **OsB** sustains a strong σ-current density circulation.[23,32] The MO-decomposed current densities and the NBO-based MCI analysis agreed that **OsB** in the S_0 state dominantly exhibits π-Hückel-type aromaticity, with a nonnegligible share of π-Craig-Möbius aromaticity. Both employed approaches agree that the aromaticity of **OsB** in the T_1 state is significantly reduced relative to the S_0 state.

The magnetically induced current densities and MCI results showed that in the S_0 state of higher members of the osmaacene series, the central Os-containing ring becomes nonaromatic, acting as a barrier between the two side polyacenic units which, on the other hand, exhibit a significant extent of π-electron delocalization. Similarly, in the T_1 state the aromaticity of the central ring becomes even more reduced relative to the S_0 state, due to more pronounced planarity distortions and the fact that unpaired electrons are localized in this ring. The localization of spin-density in the T_1 state of osmaacenes can be rationalized by means of antiaromatic Baird resonant structures, which indicated very similar localization patterns as in the T_1 state of acenes. The main difference is that in osmaacenes the spin density is even more "localized" in the central rings due to the ability of the [Os] fragment to accept the unpaired electrons.

ASSOCIATED CONTENT

Supporting Information. Optimized geometries, current density maps, MCI values, NPA results and coordinates of the optimized geometries of the studied molecules (PDF). This information is available free of charge via the Internet at http://pubs.acs.org.

AUTHOR INFORMATION

Corresponding Authors

*E-mail address: **slavkoradenkovic@kg.ac.rs; miquel.sola@udg.edu**

Notes

The authors declare no competing financial interest.

ACKNOWLEDGMENTS

The work has been performed under the Project HPC-EUROPA3 (INFRAIA-2016-1-730897), with the support of the EC Research Innovation Action under the H2020 Programme; S. R. gratefully acknowledges the support of Prof. Miquel Solà and Institute of Computational Chemistry and Catalysis and Department of Chemistry, University of Girona and the computer resources and technical support provided by Barcelona Supercomputing Center (BSC). S. R. also thanks the Serbian Ministry of Education, Science and Technological Development (Agreement No. 451-03-47/2023-01/200122) for partial support of this work. M. S. is grateful for the financial support from the Ministerio de Ciencia e Innovación (PID2020-113711GB-I00) and the Generalitat de Catalunya (Project 2021-SGR-623).

References

(1) Bleeke, J. R. Metallabenzenes. *Chem. Rev.* **2001**, *101* (5), 1205–1228. https://doi.org/10.1021/cr990337n.
(2) Thorn, D.; Hoffmann, R. Delocalization in Metallocycles. *Nouv. J. Chim.* **1979**, *3*, 39–45.
(3) Elliott, G. P.; Roper, W. R.; Waters, J. M. Metallacyclohexatrienes or 'Metallabenzenes.' Synthesis of Osmabenzene Derivatives and X-Ray Crystal Structure of [Os(CSCHCHCHCH)(CO)(PPh3)2]. *J. Chem. Soc. Chem. Commun.* **1982**, No. 14, 811–813. https://doi.org/10.1039/C39820000811.

(4) Frogley, B. J.; Wright, L. J. Fused-Ring Metallabenzenes. *Coord. Chem. Rev.* **2014**, *270–271*, 151–166. https://doi.org/https://doi.org/10.1016/j.ccr.2014.01.019.
(5) Fernández, I.; Frenking, G.; Merino, G. Aromaticity of Metallabenzenes and Related Compounds. *Chem. Soc. Rev.* **2015**, *44* (18), 6452–6463. https://doi.org/10.1039/C5CS00004A.
(6) Frogley, B. J.; Wright, L. J. Recent Advances in Metallaaromatic Chemistry. *Chem. – A Eur. J.* **2018**, *24* (9), 2025–2038. https://doi.org/10.1002/chem.201704888.
(7) Chen, D.; Xie, Q.; Zhu, J. Unconventional Aromaticity in Organometallics: The Power of Transition Metals. *Acc. Chem. Res.* **2019**, *52* (5), 1449–1460. https://doi.org/10.1021/acs.accounts.9b00092.
(8) Chen, D.; Hua, Y.; Xia, H. Metallaaromatic Chemistry: History and Development. *Chem. Rev.* **2020**, *120* (23), 12994–13086. https://doi.org/10.1021/acs.chemrev.0c00392.
(9) Chen, Z.-N.; Fu, G.; Zhang, I. Y.; Xu, X. Understanding the Nonplanarity in Aromatic Metallabenzenes: A σ-Control Mechanism. *Inorg. Chem.* **2018**, *57* (15), 9205–9214. https://doi.org/10.1021/acs.inorgchem.8b01213.
(10) Wu, J.; An, K.; Sun, T.; Fan, J.; Zhu, J. To Be Bridgehead or Not to Be? This Is a Question of Metallabicycles on the Interplay between Aromaticity and Ring Strain. *Organometallics* **2017**, *36* (24), 4896–4900. https://doi.org/10.1021/acs.organomet.7b00758.
(11) Islas, R.; Poater, J.; Solà, M. Analysis of the Aromaticity of Five-Membered Heterometallacycles Containing Os, Ru, Rh, and Ir. *Organometallics* **2014**, *33* (7), 1762–1773. https://doi.org/10.1021/om500119c.
(12) Esteruelas, M. A.; Fernández, I.; García-Yebra, C.; Martín, J.; Oñate, E. Cycloosmathioborane Compounds: Other Manifestations of the Hückel Aromaticity. *Inorg. Chem.* **2019**, *58* (4), 2265–2269. https://doi.org/10.1021/acs.inorgchem.8b03366.
(13) Buil, M. L.; Esteruelas, M. A.; Oñate, E.; Picazo, N. R. Osmathiazole Ring: Extrapolation of an Aromatic Purely Organic System to Organometallic Chemistry. *Organometallics* **2023**, *42* (4), 327–338. https://doi.org/10.1021/acs.organomet.2c00631.
(14) Haake, P.; Cronin, P. A. Aromaticity of Five- Membered Rings Containing Platinum(II). *Inorg. Chem.* **1963**, *2* (4), 879–880. https://doi.org/10.1021/ic50008a062.
(15) Qiu, R.; Wu, J.; Zhu, J. Stabilizing a 20-Electron Metallaazulyne by Aromaticity. *Inorg. Chem.* **2022**, *61* (24), 9073–9081. https://doi.org/10.1021/acs.inorgchem.2c00594.
(16) Solà, M. Aromaticity Rules. *Nat. Chem.* **2022**, *14* (6), 585–590. https://doi.org/10.1038/s41557-022-00961-w.
(17) Tkachenko, N. V; Muñoz-Castro, A.; Boldyrev, A. I. Occurrence of Double Bond in π-Aromatic Rings: An Easy Way to Design Doubly Aromatic Carbon-Metal Structures. *Molecules*. 2021. https://doi.org/10.3390/molecules26237232.
(18) El-Hamdi, M.; El Bakouri El Farri, O.; Salvador, P.; Abdelouahid, B. A.; El Begrani, M. S.; Poater, J.; Solà, M. Analysis of the Relative Stabilities of Ortho, Meta, and Para MClY(XC4H4)(PH3)2 Heterometallabenzenes (M = Rh, Ir; X = N, P; Y = Cl and M = Ru, Os; X = N, P; Y = CO). *Organometallics* **2013**, *32* (17), 4892–4903. https://doi.org/10.1021/om400629w.
(19) Szczepanik, D. W.; Andrzejak, M.; Dominikowska, J.; Pawełek, B.; Krygowski, T. M.; Szatylowicz, H.; Solà, M. The Electron Density of Delocalized Bonds (EDDB) Applied for Quantifying Aromaticity. *Phys. Chem. Chem. Phys.* **2017**, *19* (42), 28970–28981. https://doi.org/10.1039/C7CP06114E.

(20) Szczepanik, D. W.; Solà, M. Electron Delocalization in Planar Metallacycles: Hückel or Möbius Aromatic? *ChemistryOpen* **2019**, *8* (2), 219–227. https://doi.org/https://doi.org/10.1002/open.201900014.
(21) Shen, T.; Chen, D.; Lin, L.; Zhu, J. Dual Aromaticity in Both the T(0) and S(1) States: Osmapyridinium with Phosphonium Substituents. *J. Am. Chem. Soc.* **2019**, *141* (14), 5720–5727. https://doi.org/10.1021/jacs.8b11564.
(22) Chen, D.; Szczepanik, D. W.; Zhu, J.; Solà, M. Probing the Origin of Adaptive Aromaticity in 16-Valence-Electron Metallapentalenes. *Chem. – A Eur. J.* **2020**, *26* (57), 12964–12971. https://doi.org/https://doi.org/10.1002/chem.202001830.
(23) Foroutan-Nejad, C.; Vícha, J.; Ghosh, A. Relativity or Aromaticity? A First-Principles Perspective of Chemical Shifts in Osmabenzene and Osmapentalene Derivatives. *Phys. Chem. Chem. Phys.* **2020**, *22* (19), 10863–10869. https://doi.org/10.1039/D0CP01481H.
(24) Chen, Z.; Wannere, C. S.; Corminboeuf, C.; Puchta, R.; Schleyer, P. von R. Nucleus-Independent Chemical Shifts (NICS) as an Aromaticity Criterion. *Chem. Rev.* **2005**, *105* (10), 3842–3888. https://doi.org/10.1021/cr030088+.
(25) Stanger, A. NICS – Past and Present. *European J. Org. Chem.* **2020**, *2020* (21), 3120–3127. https://doi.org/https://doi.org/10.1002/ejoc.201901829.
(26) Puchta, R.; Đorđević, S.; Radenković, S.; Jiao, H.; Van Eikema Hommes, N. 25 Years of NICS – Much More than Nothing! *J. Serbian Chem. Soc.* **2022**, *87* (12), 1439–1446. https://doi.org/10.2298/JSC211203057P.
(27) Paneque, M.; Posadas, C. M.; Poveda, M. L.; Rendón, N.; Salazar, V.; Oñate, E.; Mereiter, K. Formation of Unusual Iridabenzene and Metallanaphthalene Containing Electron-Withdrawing Substituents. *J. Am. Chem. Soc.* **2003**, *125* (33), 9898–9899. https://doi.org/10.1021/ja035655p.
(28) Frogley, B. J.; Wright, L. J. A Metallaanthracene and Derived Metallaanthraquinone. *Angew. Chemie Int. Ed.* **2017**, *56* (1), 143–147. https://doi.org/10.1002/anie.201608500.
(29) Pino-Rios, R.; Báez-Grez, R.; Solà, M. Acenes and Phenacenes in Their Lowest-Lying Triplet States. Does Kinked Remain More Stable than Straight? *Phys. Chem. Chem. Phys.* **2021**, *23* (24), 13574–13582. https://doi.org/10.1039/D1CP01441B.
(30) Hoffmann, R. Building Bridges Between Inorganic and Organic Chemistry (Nobel Lecture). *Angew. Chemie Int. Ed. English* **1982**, *21* (10), 711–724. https://doi.org/https://doi.org/10.1002/anie.198207113.
(31) An, K.; Zhu, J. Predicting an Unconventional Facile Route to Metallaanthracenes. *Dalt. Trans.* **2018**, *47* (16), 5575–5581. https://doi.org/10.1039/C8DT00455B.
(32) Cuyacot, B. J. R.; Badri, Z.; Ghosh, A.; Foroutan-Nejad, C. Metallaaromaticity – a Protean World. *Phys. Chem. Chem. Phys.* **2022**, *24* (45), 27957–27963. https://doi.org/10.1039/D2CP04846A.
(33) Karadakov, P. B. Ground- and Excited-State Aromaticity and Antiaromaticity in Benzene and Cyclobutadiene. *J. Phys. Chem. A* **2008**, *112* (31), 7303–7309. https://doi.org/10.1021/jp8037335.
(34) Rosenberg, M.; Dahlstrand, C.; Kilså, K.; Ottosson, H. Excited State Aromaticity and Antiaromaticity: Opportunities for Photophysical and Photochemical Rationalizations. *Chem. Rev.* **2014**, *114* (10), 5379–5425. https://doi.org/10.1021/cr300471v.
(35) Yan, J.; Slanina, T.; Bergman, J.; Ottosson, H. Photochemistry Driven by Excited-State Aromaticity Gain or Antiaromaticity Relief. *Chem. – A Eur. J.* **2023**, *n/a* (n/a), e202203748. https://doi.org/https://doi.org/10.1002/chem.202203748.

(36) Lazzeretti, P. Assessment of Aromaticity via Molecular Response Properties. *Phys. Chem. Chem. Phys.* **2004**, *6* (2), 217–223. https://doi.org/10.1039/B311178D.
(37) Sundholm, D.; Fliegl, H.; Berger, R. J. F. Calculations of Magnetically Induced Current Densities: Theory and Applications. *Wiley Interdiscip. Rev. Comput. Mol. Sci.* **2016**, *6* (6), 639–678. https://doi.org/10.1002/wcms.1270.
(38) Sundholm, D.; Dimitrova, M.; Berger, R. J. F. Current Density and Molecular Magnetic Properties. *Chem. Commun.* **2021**, *57* (93), 12362–12378. https://doi.org/10.1039/D1CC03350F.
(39) Feixas, F.; Matito, E.; Poater, J.; Solà, M. Quantifying Aromaticity with Electron Delocalisation Measures. *Chem. Soc. Rev.* **2015**, *44* (18), 6434–6451. https://doi.org/10.1039/c5cs00066a.
(40) Keith, T. A.; Bader, R. F. W. Calculation of Magnetic Response Properties Using a Continuous Set of Gauge Transformations. *Chem. Phys. Lett.* **1993**, *210* (1–3), 223–231. https://doi.org/https://doi.org/10.1016/0009-2614(93)89127-4.
(41) Keith, T. A.; Bader, R. F. W. Topological Analysis of Magnetically Induced Molecular Current Distributions. *J. Chem. Phys.* **1993**, *99* (5), 3669–3682. https://doi.org/http://dx.doi.org/10.1063/1.466165.
(42) Lazzeretti, P.; Malagoli, M.; Zanasi, R. Computational Approach to Molecular Magnetic Properties by Continuous Transformation of the Origin of the Current Density. *Chem. Phys. Lett.* **1994**, *220* (3–5), 299–304. https://doi.org/https://doi.org/10.1016/0009-2614(94)00158-8.
(43) Steiner, E.; Fowler, P. W. Patterns of Ring Currents in Conjugated Molecules: A Few-Electron Model Based on Orbital Contributions. *J. Phys. Chem. A* **2001**, *105* (41), 9553–9562. https://doi.org/10.1021/jp011955m.
(44) te Velde, G.; Bickelhaupt, F. M.; Baerends, E. J.; Fonseca Guerra, C.; van Gisbergen, S. J. A.; Snijders, J. G.; Ziegler, T. Chemistry with ADF. *J. Comput. Chem.* **2001**, *22* (9), 931–967. https://doi.org/https://doi.org/10.1002/jcc.1056.
(45) Grimme, S.; Antony, J.; Ehrlich, S.; Krieg, H. A Consistent and Accurate Ab Initio Parametrization of Density Functional Dispersion Correction (DFT-D) for the 94 Elements H-Pu. *J. Chem. Phys.* **2010**, *132* (15), 154104. https://doi.org/10.1063/1.3382344.
(46) Grimme, S.; Ehrlich, S.; Goerigk, L. Effect of the Damping Function in Dispersion Corrected Density Functional Theory. *J. Comput. Chem.* **2011**, *32* (7), 1456–1465. https://doi.org/https://doi.org/10.1002/jcc.21759.
(47) Lenthe, E. van; Baerends, E. J.; Snijders, J. G. Relativistic Regular Two-component Hamiltonians. *J. Chem. Phys.* **1993**, *99* (6), 4597–4610. https://doi.org/10.1063/1.466059.
(48) van Lenthe, E.; van Leeuwen, R.; Baerends, E. J.; Snijders, J. G. Relativistic Regular Two-Component Hamiltonians. *Int. J. Quantum Chem.* **1996**, *57* (3), 281–293. https://doi.org/https://doi.org/10.1002/(SICI)1097-461X(1996)57:3<281::AID-QUA2>3.0.CO;2-U.
(49) Ayachit, U. *The ParaView Guide: A Parallel Visualization Application*; Kitware, 2015.
(50) Jusélius, J.; Sundholm, D.; Gauss, J. Calculation of Current Densities Using Gauge-Including Atomic Orbitals. *J. Chem. Phys.* **2004**, *121* (9), 3952–3963. https://doi.org/http://dx.doi.org/10.1063/1.1773136.
(51) Irons, T. J. P.; Spence, L.; David, G.; Speake, B. T.; Helgaker, T.; Teale, A. M. Analyzing Magnetically Induced Currents in Molecular Systems Using Current-Density-Functional

Theory. *J. Phys. Chem. A* **2020**, *124* (7), 1321–1333. https://doi.org/10.1021/acs.jpca.9b10833.
(52) Elhay, S.; Kautsky, J. Algorithm 655: IQPACK: FORTRAN Subroutines for the Weights of Interpolatory Quadratures. *ACM Trans. Math. Softw.* **1987**, *13* (4), 399–415. https://doi.org/10.1145/35078.214351.
(53) Giambiagi, M.; de Giambiagi, M. S.; dos Santos Silva, C. D.; de Figueiredo, A. P. Multicenter Bond Indices as a Measure of Aromaticity. *Phys. Chem. Chem. Phys.* **2000**, *2* (15), 3381–3392. https://doi.org/http://dx.doi.org/10.1039/B002009P.
(54) Bultinck, P.; Ponec, R.; Van Damme, S. Multicenter Bond Indices as a New Measure of Aromaticity in Polycyclic Aromatic Hydrocarbons. *J. Phys. Org. Chem.* **2005**, *18* (8), 706–718. https://doi.org/10.1002/poc.922.
(55) Bochicchio, R.; Ponec, R.; Torre, A.; Lain, L. Multicenter Bonding within the AIM Theory. *Theor. Chem. Acc.* **2001**, *105* (4), 292–298. https://doi.org/10.1007/s002140000236.
(56) Heyndrickx, W.; Salvador, P.; Bultinck, P.; Solà, M.; Matito, E. Performance of 3D-Space-Based Atoms-in-Molecules Methods for Electronic Delocalization Aromaticity Indices. *J. Comput. Chem.* **2011**, *32* (3), 386–395. https://doi.org/10.1002/jcc.21621.
(57) Bultinck, P.; Rafat, M.; Ponec, R.; Van Gheluwe, B.; Carbó-Dorca, R.; Popelier, P. Electron Delocalization and Aromaticity in Linear Polyacenes: Atoms in Molecules Multicenter Delocalization Index. *J. Phys. Chem. A* **2006**, *110* (24), 7642–7648. https://doi.org/10.1021/jp0609176.
(58) Foster, J. P.; Weinhold, F. Natural Hybrid Orbitals. *J. Am. Chem. Soc.* **1980**, *102* (24), 7211–7218. https://doi.org/10.1021/ja00544a007.
(59) Frisch, M. J.; Trucks, G. W.; Schlegel, H. B.; Scuseria, G. E.; Robb, M. A.; Cheeseman, J. R.; Scalmani, G.; Barone, V.; Mennucci, B.; Petersson, G. A.; Nakatsuji, H.; Caricato, M.; Li, X.; Hratchian, H. P.; Izmaylov, A. F.; Bloino, J.; Zheng, G.; Sonnenberg, J. L.; Hada, M.; Ehara, M.; Toyota, K.; Fukuda, R.; Hasegawa, J.; Ishida, M.; Nakajima, T.; Honda, Y.; Kitao, O.; Nakai, H.; Vreven, T.; Montgomery, J. A.; Peralta, J. E.; Ogliaro, F.; Bearpark, M.; Heyd, J. J.; Brothers, E.; Kudin, K. N.; Staroverov, V. N.; Kobayashi, R.; Normand, J.; Raghavachari, K.; Rendell, A.; Burant, J. C.; Iyengar, S. S.; Tomasi, J.; Cossi, M.; Rega, N.; Millam, J. M.; Klene, M.; Knox, J. E.; Cross, J. B.; Bakken, V.; Adamo, C.; Jaramillo, J.; Gomperts, R.; Stratmann, R. E.; Yazyev, O.; Austin, A. J.; Cammi, R.; Pomelli, C.; Ochterski, J. W.; Martin, R. L.; Morokuma, K.; Zakrzewski, V. G.; Voth, G. A.; Salvador, P.; Dannenberg, J. J.; Dapprich, S.; Daniels, A. D.; Farkas; Foresman, J. B.; Ortiz, J. V; Cioslowski, J.; Fox, D. J. Gaussian 09, Revision B.01. *Gaussian Inc., Wallingford CT*. Wallingford CT 2009.
(60) Antić, M.; Furtula, B.; Radenković, S. Aromaticity of Nonplanar Fully Benzenoid Hydrocarbons. *J. Phys. Chem. A* **2017**, *121* (18), 3616–3626. https://doi.org/10.1021/acs.jpca.7b02521.
(61) Radenković, S.; Gutman, I.; Bultinck, P. Comparative Study of Aromaticity in Tetraoxa[8]Circulenes. *J. Phys. Chem. A* **2012**, *116* (37), 9421–9430. https://doi.org/10.1021/jp307281y.
(62) Bendikov, M.; Duong, H. M.; Starkey, K.; Houk, K. N.; Carter, E. A.; Wudl, F. Oligoacenes: Theoretical Prediction of Open-Shell Singlet Diradical Ground States. *J. Am. Chem. Soc.* **2004**, *126* (24), 7416–7417. https://doi.org/10.1021/ja048919w.
(63) Poater, J.; Bofill, J. M.; Alemany, P.; Solà, M. Local Aromaticity of the Lowest-Lying

Singlet States of [n]Acenes (n = 6−9). *J. Phys. Chem. A* **2005**, *109* (47), 10629–10632. https://doi.org/10.1021/jp055188t.
(64) Proos Vedin, N.; Escayola, S.; Radenković, S.; Solà, M.; Ottosson, H. The Lowest Nπ* States of Heteroaromatics: When and in What Way Are They Aromatic or Antiaromatic? *Prep.*
(65) Mandado, M.; Graña, A. M.; Pérez-Juste, I. Aromaticity in Spin-Polarized Systems: Can Rings Be Simultaneously Alpha Aromatic and Beta Antiaromatic? *J. Chem. Phys.* **2008**, *129* (16), 164114. https://doi.org/10.1063/1.2999562.
(66) Gu, X.; Yang, L.; Jin, P. Planar Inorganic Five-Membered Heterocycles with σ + π Dual Aromaticity in Both S0 and T1 States. *Phys. Chem. Chem. Phys.* **2022**, *24* (36), 22091–22101. https://doi.org/10.1039/D2CP03116G.
(67) Szczepanik, D. W.; Solà, M.; Andrzejak, M.; Pawełek, B.; Dominikowska, J.; Kukułka, M.; Dyduch, K.; Krygowski, T. M.; Szatylowicz, H. The Role of the Long-Range Exchange Corrections in the Description of Electron Delocalization in Aromatic Species. *J. Comput. Chem.* **2017**, *38* (18), 1640–1654. https://doi.org/https://doi.org/10.1002/jcc.24805.
(68) Chai, J.-D.; Head-Gordon, M. Long-Range Corrected Hybrid Density Functionals with Damped Atom–Atom Dispersion Corrections. *Phys. Chem. Chem. Phys.* **2008**, *10* (44), 6615–6620. https://doi.org/10.1039/B810189B.
(69) Alvarado-Soto, L.; Ramírez-Tagle, R.; Arratia-Pérez, R. Spin–Orbit Effects on the Aromaticity of the Re3Cl9 and Re3Br9 Clusters. *Chem. Phys. Lett.* **2008**, *467* (1), 94–96. https://doi.org/https://doi.org/10.1016/j.cplett.2008.11.020.
(70) Schott, E.; Zárate, X.; Arratia-Pérez, R. Relativistic Scalar and Spin–Orbit Density Functional Calculations of the Electronic Structure, NICS Index and ELF Function of the [Re2(CO)8(μ-BiPh)2] and [Re2(CO)8(μ-BiPh2)2] Clusters. *Polyhedron* **2011**, *30* (5), 846–850. https://doi.org/https://doi.org/10.1016/j.poly.2010.12.022.

Table of Contents Graphic

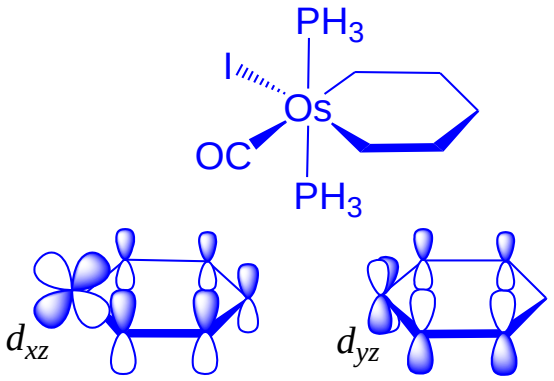

		π Hückel	π Craig-Möbius
S_0		91% aromaticity	9% aromaticity
T_1	α	48% aromaticity	52% antiaromaticity
	β	92% aromaticity	8% aromaticity

The aromatic character of osmaacenes in their lowest-lying singlet and triplet states was examined by means of the magnetically induced current densities and multicentre delocalization indices. Contrary to benzene, which is antiaromatic in the T_1 state, osmabenzene molecule preserves some of its aromaticity in the T_1 state. In higher osmaacenes in the S_0 and T_1 states, the central Os-containing ring becomes nonaromatic, acting as a barrier between the two aromatic polyacenic units.